

CEBSNet: Change-Excited and Background-Suppressed Network with Temporal Dependency Modeling for Bitemporal Change Detection

Qi'ao Xu^{a,1}, Yan Xing^{b,1}, Jiali Hu^a, Yunan Jia^a and Rui Huang^{a,*}

^aCollege of Computer Science and Technology, Civil Aviation University of China, Tianjin, 300300, China

^bCollege of Safety Science and Engineering, Civil Aviation University of China, Tianjin, 300300, , China

ARTICLE INFO

Keywords:

Change detection
Remote sensing
Temporal dependency
Feature excitation and suppression
Attention mechanism

ABSTRACT

Change detection, a critical task in remote sensing and computer vision, aims to identify pixel-level differences between image pairs captured at the same geographic area but different times. It faces numerous challenges such as illumination variation, seasonal changes, background interference, and shooting angles, especially with a large time gap between images. While current methods have advanced, they often overlook temporal dependencies and overemphasize prominent changes while ignoring subtle but equally important changes. To address these limitations, we introduce **CEBSNet**, a novel change-excited and background-suppressed network with temporal dependency modeling for change detection. During the feature extraction, we utilize a simple Channel Swap Module (CSM) to model temporal dependency, reducing differences and noise. The Feature Excitation and Suppression Module (FESM) is developed to capture both obvious and subtle changes, maintaining the integrity of change regions. Additionally, we design a Pyramid-Aware Spatial-Channel Attention module (PASCA) to enhance the ability to detect change regions at different sizes and focus on critical regions. We conduct extensive experiments on three common street view datasets and two remote sensing datasets, and our method achieves the state-of-the-art performance.

1. Introduction

Change detection (CD) focuses on detecting pixel-level changes in image pairs captured at the same location but different times [2]. These techniques have widespread applications in various fields, such as disaster monitoring and assessment, urban planning and development, natural resource monitoring and utilization, farmland surveys, traffic regulation, and remote sensing [7, 15]. As sensor technology advances, the complexity of image pairs has notably increased. Traditional methods mostly rely on image information like gray-scale/color, texture, and shape, which makes it difficult to handle complex noise interferences and severely limits detection performance [33]. Recently, deep learning-based CD methods have gained widespread attention due to their robust feature representation capabilities, which effectively reducing noise interference [3].

Despite the notable progress, current CD methods still face critical challenges when applied to complex scenarios. The primary challenge stems from the substantial noise interference caused by temporal differences. As shown in Figure 1, this limitation manifests in two key aspects: 1) **Susceptibility to various noise**: Image pairs are highly vulnerable to factors such as illumination variation, seasonal changes, background interference, and shooting angles, leading to reduced detection precision and limited cross-scenario adaptability. 2) **Neglect of subtle changes**: Most models focus on detecting obvious changes while

overlooking subtle changes, resulting in missed detections and constrained minor-change detection capability.

We contend that the underlying reasons for the subpar performance are the low-quality change features, arising from two main factors: 1) **Temporal dependency neglect**: Siamese networks treat image pairs as temporally independent entities, failing to capture latent temporal dependencies. Significant inter-pair discrepancies lead to noise susceptibility and inaccurate change detection. 2) **Imbalanced focus on change regions**: Excessive attention to prominent changes causes neglect of subtle yet critical changes, substantially increasing missed detection rates. Modeling the temporal dependency between image pairs seems promising. It can reduce noise and differences, improving detection performance. But it may weaken the distinct changes between pairs and still miss subtle changes due to the long-standing bias.

To tackle the aforementioned issues, we present **CEBSNet**, a novel change-excited and background-suppressed network with temporal dependency modeling for change detection. It utilizes a simple Channel Swap Module (CSM) to model the potential temporal dependency between image pairs during feature extraction, alleviating differences and noise interference. The Feature Excitation and Suppression Module (FESM) capture both prominent and subtle changes by exciting change-related regions and suppressing background noise. Moreover, a Pyramid-Aware Spatial-Channel Attention module (PASCA) is developed. By leveraging multi-scale receptive fields and attention mechanisms, this combination effectively boosts the ability to detect change objects at various scales. We conduct extensive experiments on five CD datasets, and our method achieves the state-of-the-art performance.

Our contributions are summarized as follows:

*Corresponding author: Rui Huang

✉ qaxu00@163.com (Q. Xu); yxing@cauc.edu.cn (Y. Xing);

rhuang@cauc.edu.cn (R. Huang)

ORCID(s): 0009-0002-5567-438X (Q. Xu)

¹These authors contributed equally to this work.

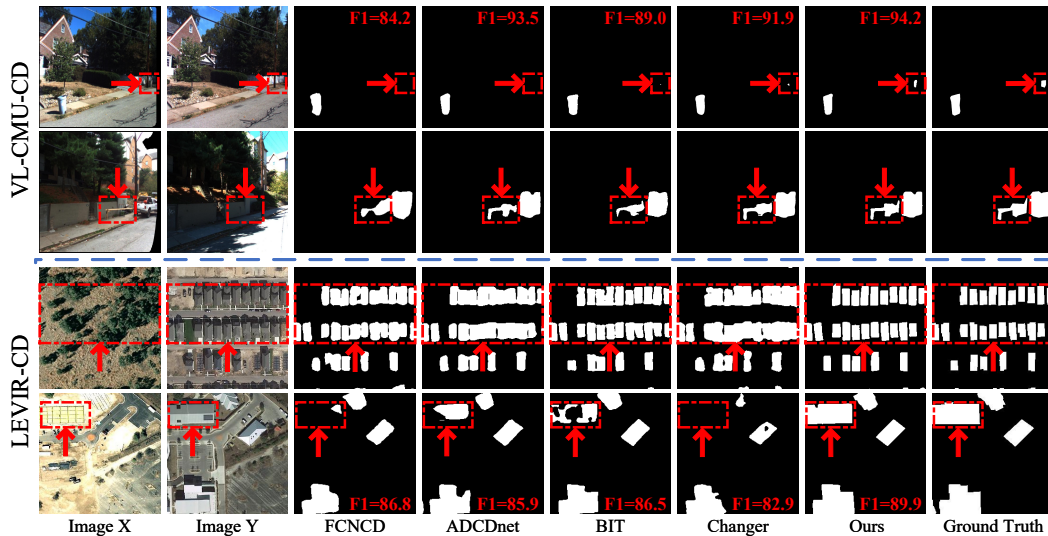


Figure 1: Motivation analysis. We compare our CEBSNet with existing CD methods on VL-CMU-CD and LEVIR-CD datasets. The objects in red dotted box are important change regions, and the F1 scores objectively measure the performance.

- We present an advanced change detection method CEBSNet. It applies a Channel Swap Module (CSM) to explore the temporal correlation between image pairs during feature extraction.
- We develop a Feature Excitation and Suppression Module (FESM) to capture both obvious and subtle changes. Additionally, a Pyramid-Aware Spatial-Channel Attention module (PASCA) is designed to aggregates change regions at various sizes.
- Extensive experiments conducted on three common street-view CD datasets and two remote sensing CD datasets demonstrate the superiority and effectiveness of our CEBSNet, validating its practical value.

The subsequent sections of this paper are organized as follows: Section 2 reviews related work on change detection along with feature excitation and suppression. Section 3 introduces the proposed CEBSNet. Section 4 presents the experimental results. Section 5 concludes with a summary.

2. Related Work

2.1. Change Detection

In recent years, change detection has gained increasing attention in computer vision. Traditional methods like Support Vector Machines (SVM), Principal Component Analysis (PCA), Gaussian Mixture Models (GMM), K-means clustering, due to their limitations, struggle to meet the current demands for high-speed and accurate detection [30].

The development and application of deep-learning technologies have revolutionized change detection. These methods, with strong learning and representation capabilities, have improved performance significantly [29]. For example, Daudt et al. [9] introduces three structures: early-fusion EC-EF, mid-fusion FC-Siam-conc and FC-Siam-diff. Huang et

al. [17] presents ADCDNet, a multi-scale change detection network that uses a siamese network to extract features and compute absolute differences for change detection. Bandara et al. [4] proposes ChangeFormer, a siamese network with a hierarchical transformer encoder. It fuses multi-scale difference features to detect changes. Fang et al. [11] proposes Changer, which processes image pairs through an encoder’s interaction-layer sequence and uses flow-based dual-alignment fusion for feature alignment. Lv et al. [23] introduces a method integrating a multi-scale attention network and change-gradient images to fuse multi-scale features for change detection. Zhao et al. [40] introduces MAPNet, a network that performs multi-scale alignment and progressive feature fusion to enhance detection performance.

Despite these advancements, most methods do not consider temporal correlation between images when extracting features. So they are easily affected by background noise. Although some methods have tried image concatenation or feature-pair fusion, the feature interaction remains insufficient. To tackle this issue, this paper proposes a simple and effective channel swap module. By exchanging feature information between image pairs, it explores their potential temporal correlation, reduces background differences and noise interference, and improves change detection accuracy.

2.2. Feature Excitation and Suppression

Feature excitation and suppression play a crucial role in deep learning by enhancing feature responses in regions of interest while suppressing irrelevant or redundant information. The attention mechanism represents the most prevalent means of achieving this objective. It has been widely applied in various fields such as natural language processing, computer vision, and time series analysis [25]. At its essence, the attention mechanism entails the learning of a set of weight coefficients. By applying these weights to features, it foregrounds crucial features and diminishes

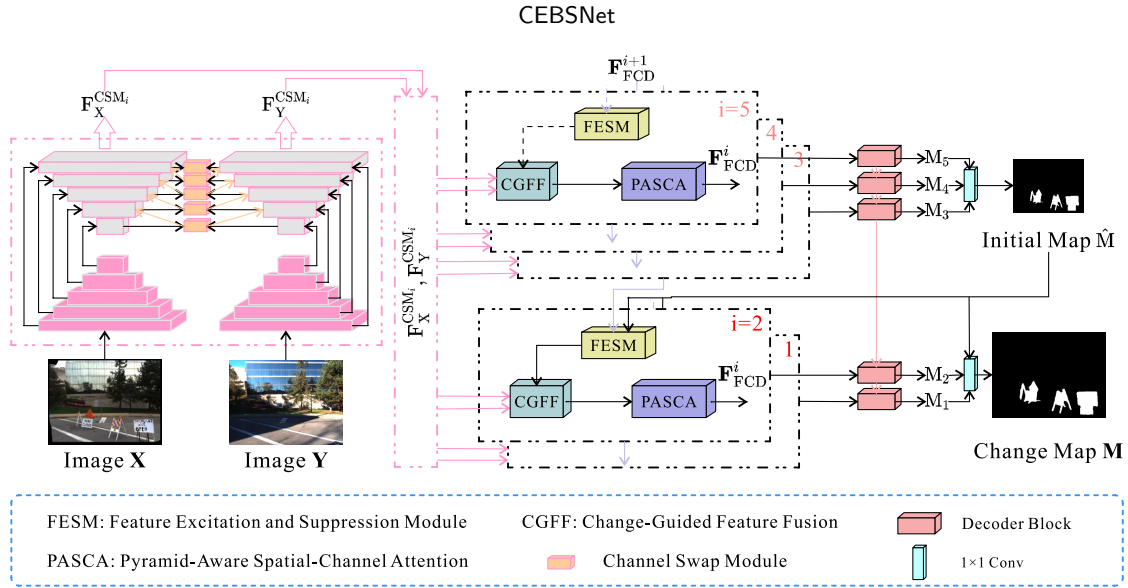


Figure 2: The architecture of our CEBSNet. It comprises three key stages: 1) Spatial-Temporal Feature Extraction, where a siamese encoder with Channel Swap Module (CSM) extracts multi-scale spatiotemporal feature pairs; 2) Change Feature Refinement, where change features are generated and iteratively refined through CGFF, FESM and PASCA; and 3) Multi-Scale Change Detection, where refined change features are decoded into multi-scale change maps and fused to generate the final change map.

the influence of unimportant ones. For instance, SENet [16] adjusts channel importance by modeling channel interdependencies, improving the network’s representation ability. Self-Attention [34] focuses on modeling global feature correlations, capturing long-range dependencies to make up for CNNs’ focus on local information. DANet [13] and CBAM [36] adjusts spatial and channel weights in both dimensions to highlight important features.

In change detection, these processes are assume a critical role. For example, STANet [5] designs a change self-attention mechanism to calculate weighted spatio-temporal dependencies for feature excitation. DMINet [12] adopts a dual-branch multi-layer spatio-temporal network with self-attention and cross-attention integration to enhance change features, addressing the issue of foreground-background imbalance. A2Net [21] uses progressive feature aggregation and a attention module to identify changes and enhances feature representation. Transformer-based methods like BIT [6], ACAHNet [39], and M-Swin [26] primarily utilize self-attention for feature extraction or spatial information modeling to highlight important change regions.

Current CD methods mainly focus on obvious change regions, often overlook less prominent but important change regions. To address this issue, this paper put forward a dual-branch feature excitation and suppression module. This module helps the network learn both obvious and subtle changes, resulting in more accurate change regions. It also solves the problem of reduced differences when modeling image temporal correlation, improving detection accuracy.

3. Methodology

3.1. Overview

As shown in Figure 2, our CEBSNet consists of three main stages: Spatial-Temporal Feature Extraction, Change Feature Refinement, and Multi-Scale Change Detection. A siamese encoder with shared weights processes the image pair \mathbf{X} and \mathbf{Y} , generating five pairs of multi-scale features $\{F_X^{CSM_i}, F_Y^{CSM_i}\}_{i=1}^5$ that encode hierarchical spatial-semantic information. Multi-scale feature pairs undergo iterative refinement through feature excitation and attention modules. The refined change features $\{F_{FCD}^i\}_{i=1}^5$ are fed into the decoder to produce multi-scale change maps $\{M_i\}_{i=1}^5$. These masks are combined to generate the final change map \mathbf{M} . For supervised training, all predicted masks are bilinearly upsampled to match the input image resolution, enabling direct loss computation and network optimization.

3.2. Spatial-Temporal Feature Extraction

The siamese network extracts multi-scale spatiotemporal features through a weight-shared VGG16_bn backbone, enhanced by a Feature Pyramid Network (FPN) and Channel Swap Module (CSM). It processes image pairs \mathbf{X} and \mathbf{Y} to generate hierarchical features $\{F_X^{CSM_i}, F_Y^{CSM_i}\}_{i=1}^5$, where FPN improves scale adaptability through lateral cross-layer fusion, and CSM enables temporal interaction via channel-wise feature recalibration. The process can be expressed as:

$$F_X^{CSM_i}, F_Y^{CSM_i} = \begin{cases} CSM(F_X^{Conv_i}, F_Y^{Conv_i}), & i = 5 \\ CSM(F_X^i, F_Y^i), & i = 4, 3, 2, 1 \end{cases} \quad (1)$$

where $CSM(\cdot, \cdot)$ denotes the channel swap operation. The intermediate features F_X^i and F_Y^i are computed as follows:

$$\begin{cases} F_X^i = \text{Conv}_2([F_X^{\text{Conv}_i}, Up(F_X^{\text{CSM}_{i+1}})], 3, 3) \\ F_Y^i = \text{Conv}_2([F_Y^{\text{Conv}_i}, Up(F_Y^{\text{CSM}_{i+1}})], 3, 3) \end{cases} \quad (2)$$

where $\text{Conv}_2(\cdot, 3, 3)$ denotes the convolution layers with two 3×3 kernels, $Up(\cdot)$ refers to bilinear upsampling, and $[\cdot, \cdot]$ indicates feature concatenation along the channel dimension.

3.2.1. Channel Swap Module (CSM)

The CSM mitigates temporal discrepancies in change detection by dynamically exchanging channel-level features between dual-temporal image pairs. Significant foreground-background differences caused by time intervals often hinder accurate feature extraction and change region detection. Traditional siamese networks, lacking explicit temporal correction modeling, exhibit suboptimal sensitivity to genuine changes. To address this, CSM employs a channel-swapping operation (Figure 3), which blends complementary temporal information while preserving dominant patterns.

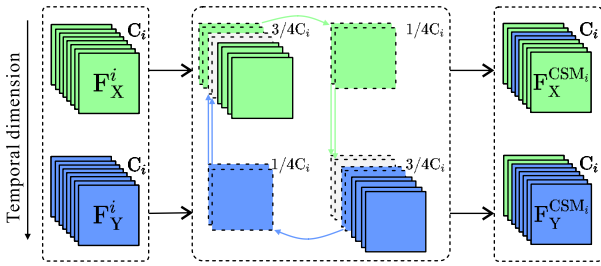


Figure 3: The architecture of CSM. It exchanges channel-level features between image pairs to model temporal dependencies.

3.3. Change Feature Refinement

The refinement stage progressively optimizes change representations through three core modules: Change-Guided Feature Fusion (CGFF), Feature Excitation and Suppression Module (FESM), and Pyramid-Aware Spatial-Channel Attention (PASCA). Specifically, the CGFF generates initial change features using deep-layer change priors for semantic guidance. The FESM dynamically reweights features to amplify change-sensitive patterns while reducing background interference, capturing both obvious and subtle changes. The PASCA employs multi-receptive fields and spatial-channel attention to focus on change regions across multiple scales.

3.3.1. Change-Guided Feature Fusion (CGFF)

As shown in Figure 4, the CGFF module adaptively fuses bi-temporal features $F_X^{\text{CSM}_i}$ and $F_Y^{\text{CSM}_i}$ under the guidance of refined change features F_{FESM}^i . The process concatenates the bi-temporal features, computes their absolute difference, and use change-guided feature fusion to generate change features. The formulations are as follows:

$$F_{\text{Con}} = \text{Conv}_2([F_X^{\text{CSM}}, F_Y^{\text{CSM}}], 1, 3) \quad (3)$$

$$F_{\text{AD}} = \text{Conv}_2(\text{abs}(F_X^{\text{CSM}} - F_Y^{\text{CSM}}), 1, 3) \quad (4)$$

$$F_{\text{CGFF}}^i = \begin{cases} F_{\text{AD}}^i, & i = 5 \\ \text{Conv}_1(F_{\text{Con}}^i + F_{\text{AD}}^i, 1), & i = 4, 3, 2, 1 \end{cases} \quad (5)$$

Here, $F_{\text{Con}}^i = \text{Conv}_2(F_{\text{Con}} \odot F_{\text{FESM}}^i, 1, 3)$, and \odot indicates element-wise multiplication. $\text{abs}(\cdot)$ is the absolute operation, $\text{Conv}_2(\cdot, 1, 3)$ denotes sequential convolution layers with kernel sizes of 1×1 and 3×3 , and $\text{Conv}_1(\cdot, 1)$ represents a 1×1 convolution layer.

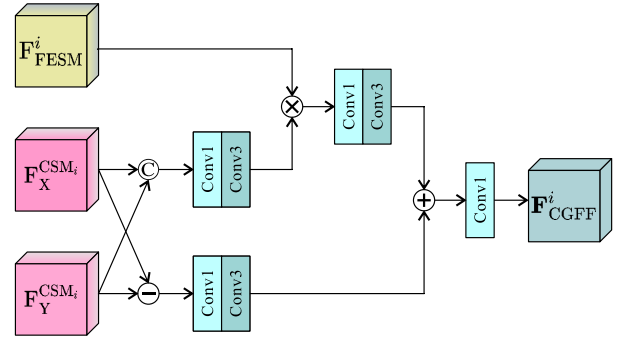


Figure 4: The architecture of CGFF. It adaptively fuses bi-temporal features guided by refined change features through bi-temporal concatenation, absolute difference computation, and change-guided feature fusion.

3.3.2. Feature Excitation and Suppression Module (FESM)

Designed to amplify both prominent and subtle change patterns while suppressing noise interference, the core innovation lies in dual-axis adaptive feature recalibration through dynamic spatial-wise importance adjustment, significantly improving sensitivity to fine-grained changes. As shown in Figure 5, FESM operates by partitioning feature maps along dual-axis to compute: ① Excitation branch: generates region-importance scores to enhance salient changes, producing activated features F_{e_out} . ② Suppression branch: calculates region-suppression scores to obtain initial suppressed features F_{s_in} , then refines them via foreground-boosting and background-suppression operations to generate F_{s_out} . The final output F_{FESM} integrates the two branches using learnable fusion weights, as expressed by:

$$F_{\text{FESM}} = \gamma \cdot F_{e_out} + (1 - \gamma) \cdot F_{s_out}, i = 4, 3, 2, 1 \quad (6)$$

where γ is an adaptive coefficient. F_{e_out} and F_{s_out} are the output features of both branches.

Excitation Branch. The branch adaptively strengthens salient change regions by applying multiple operations on features F_A , whose formulation varies across different layers:

$$F_A^i = \begin{cases} F_{\text{PASCA}}^{i+1}, & i = 4, 3 \\ Up(\text{Conv}_2(\hat{M}_c + F_A^i, 1, 3)), & i = 2, 1 \end{cases} \quad (7)$$

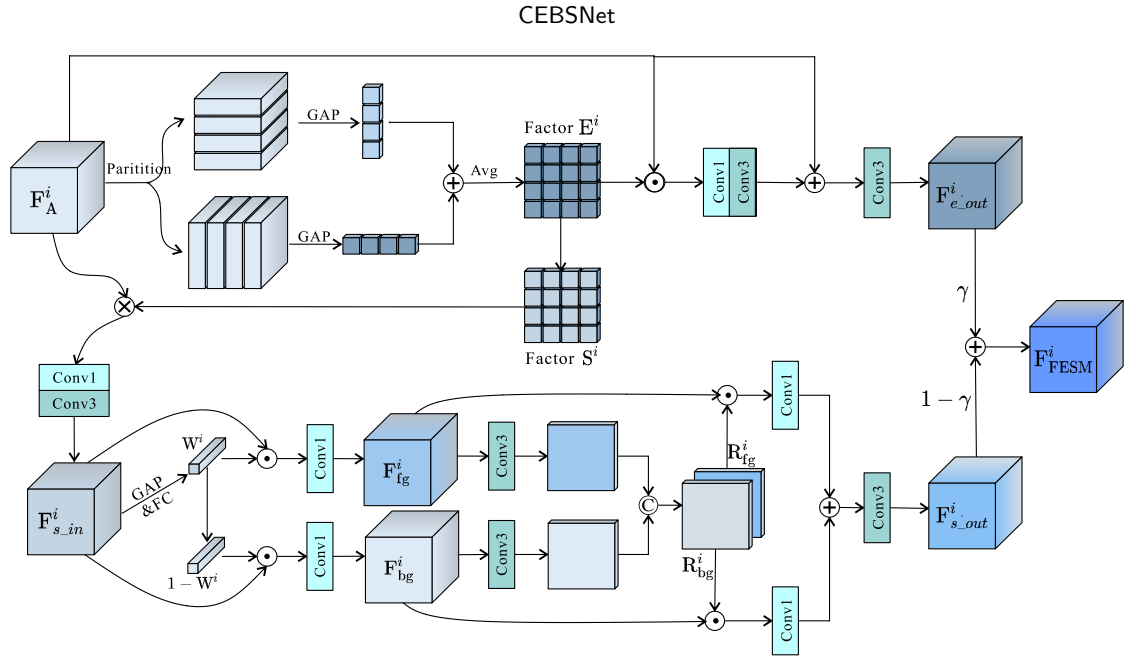


Figure 5: The architecture of FESM. It consists of two branches: the excitation branch enhances prominent change regions, while the suppression branch captures subtle changes by boosting foreground and suppressing background.

Here, $F_A^i = \text{Conv}_1(\hat{M}_c \odot \text{Conv}_1(F_{\text{PASCAS}}^{i+1}, 3), 3)$, and $\hat{M}_c = \text{Conv}_1(\hat{M}, 1)$. $\text{Conv}_1(\cdot, 3)$ denotes a 3×3 convolution layer, and \hat{M} is the initial change map.

Dual-Axis Partitioning: Feature F_A is partitioned into k sub-regions along both the horizontal and vertical axes. The region-importance scores $E \in R^{k \times k}$ are computed as:

$$\begin{cases} E_W = SF(GAP(\text{Conv}_1(S_W(F_A, k), 1))) \\ E_H = SF(GAP(\text{Conv}_1(S_H(F_A, k), 1))) \end{cases} \quad (8)$$

$$E = \frac{E_W + E_H}{2} \quad (9)$$

where $S_W(\cdot, k)$ and $S_H(\cdot, k)$ are horizontal and vertical splitting operations dividing F_A into k sub-regions. $GAP(\cdot)$ denotes global average pooling, and $SF(\cdot)$ represents Soft-max normalization. k is the partition factor.

Feature Modulation: The importance matrix E modulates feature responses to generate F_{e_out} by:

$$F_{e_out} = \text{Conv}_1(F_A + \text{Conv}_2(E \odot F_A, 1, 3), 3). \quad (10)$$

Suppression Branch The suppression branch selectively suppresses the salient change regions using a suppression score S , resulting in a feature map F_{s_in} that focuses on non-salient regions:

$$F_{s_in} = \text{Conv}_2(F_A \odot S, 1, 3) \quad (11)$$

The region-suppression matrix $S \in R^{k \times k}$ is derived from E to suppress high-score regions, highlighting regions with relatively lower scores. It is computed as:

$$s_{mn} = \begin{cases} 1 - \beta, & \text{if } e_{mn} = \max(E) \\ 1, & \text{otherwise} \end{cases} \quad (12)$$

where $\beta \in [0, 1]$ controls suppression intensity, and e_{mn} is the score of the (m, n) -th sub-region in E .

Foreground-Background Disentanglement: The channel-wise attention weight W is computed by:

$$W = SG(\text{Conv}_1(GAP(F_{s_in}), 1)) \quad (13)$$

where $SG(\cdot)$ is sigmoid function. The F_{s_in} are decomposed into foreground and background features F_{fg} and F_{bg} as:

$$\begin{cases} F_{fg} = F_{s_in} \odot W \\ F_{bg} = F_{s_in} \odot (1 - W) \end{cases} \quad (14)$$

Feature Recalibration: The excitation factor R_{fg} and background suppression factor R_{bg} are obtained by:

$$R_{fg}, R_{bg} = SF([\text{Conv}_1(F_{fg}, 1), \text{Conv}_1(F_{bg}, 1)]) \quad (15)$$

The suppression output F_{s_out} combines both paths:

$$F_{s_out} = \text{Conv}_1(F_{fg} \odot R_{fg} + F_{bg} \odot R_{bg}, 3) \quad (16)$$

3.3.3. Pyramid-Aware Spatial-Channel Attention (PASCA)

The PASCA effectively enhances the network's ability to perceive change regions across different scales by integrating multi-scale pyramid enhancement and spatial-channel attention mechanisms, as illustrated in Figure 6.

Multi-Scale Pyramid Enhancement. Convolutions and consecutive max-pooling operations are applied on F_{CGFF} to extract multi-scale features, yielding F_{MSPE} , as follows:

$$F_{in} = \text{Conv}_3(F_{\text{CGFF}}, 1, 3, 1) \quad (17)$$

$$F_{\text{MSPE}} = \text{Conv}_2([F_{in}, F_{\text{MP}_1}, F_{\text{MP}_2}, F_{\text{MP}_3}], 1, 3) \quad (18)$$

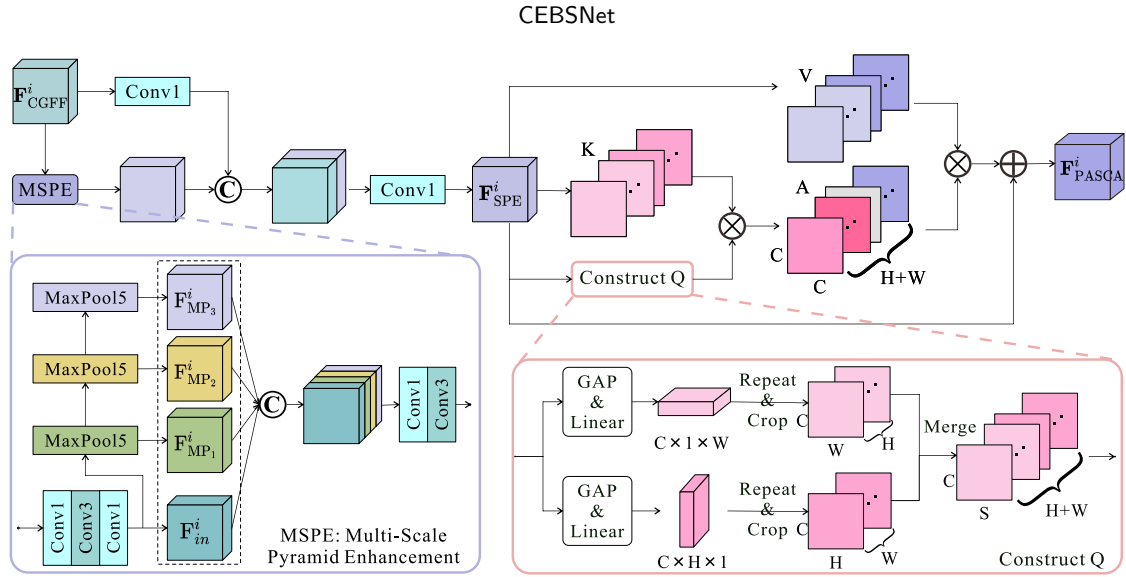


Figure 6: The architecture of PASCA. It enhances multi-scale change detection via pyramid-based feature fusion and spatial-channel attention, enabling localization of changes at various scales.

where $\text{Conv}_3(\cdot, 1, 3, 1)$ denotes sequential convolutions with kernel sizes of 1×1 , 3×3 , and 1×1 . $F_{MP_1}, F_{MP_2}, F_{MP_3}$ are the outputs of one, two and three max-pooling layers, respectively.

To preserve the original information, a residual branch combines the original features with F_{MSPE} to produce F_{SPE} :

$$F_{SPE} = \text{Conv}_1([F_{MSPE}, \text{Conv}_1(F_{CGFF}, 1)], 1) \quad (19)$$

Spatial-Channel Attention (SCA). The SCA [31] is applied on F_{SPE} to generate the refined F_{PASCA} , adaptively emphasizing crucial change regions. By jointly modeling spatial and channel information, it avoids overlooking small objects (from channel-only modeling) and disrupting large objects (from spatial-only modeling). The process is expressed as:

$$F_{PASCA} = F_{SPE} + \gamma \cdot \left(\sum_{m=1}^C A_m \cdot V \right) \quad (20)$$

where γ is a learnable parameter. The features Q , K , and V are constructed from F_{SPE} with $Q = K = V \in \mathbb{R}^{(H+W) \times C \times S}$, where $S = H = W$. The attention weight matrix A is calculated as:

$$A_{m,n} = \frac{\exp(Q_m \cdot K_n^T)}{\sum_{m=1}^C \exp(Q_m \cdot K_n^T)}, m, n \in 1, 2, \dots, C \quad (21)$$

where $A_{m,n}$ reflects channel-wise relative attention weights. The construction process of Q , K , and V is designed to enrich feature representation by capturing information in both spatial and channel dimensions. Specifically, the input feature F_{SPE} is segmented along the height (H) and width (W) dimensions, yielding two groups of slices: H slices of size $C \times W$ and W slices of size $C \times H$. Since $H = W$, these slices are stacked and fused to obtain $Q = K = V \in \mathbb{R}^{(H+W) \times C \times S}$.

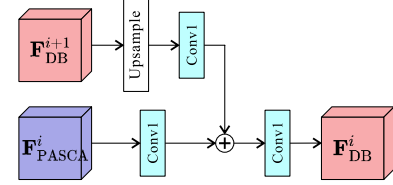


Figure 7: The architecture of DB. It propagates semantic-rich deep features to shallow layers via cross-scale fusion, integrating global context while retaining spatial details.

By integrating multi-scale aggregation and attention mechanisms, the PASCA effectively utilizes information at different scales and highlights change regions, ensuring robust and accurate change detection.

3.4. Multi-Scale Change Detector

The change detector hierarchically fuses refined change features across multiple scales to generate final change maps. As shown in Figure 2, it uses five decoder blocks to progressively enhance features and predict change masks at different scales.

3.4.1. Decoder Block

Each decoder block propagates semantic-rich deep features to adjacent shallow layers through cross-scale fusion, leveraging global context while preserving spatial details. As illustrated in Figure 7, the high-level features F_{DB}^{i+1} are unsampled and added to shallow features F_{PASCA}^i :

$$F_{DB}^i = \begin{cases} \text{Conv}_1(F_{PASCA}^5, 1), & i = 5 \\ \text{Conv}_1(\text{Conv}_1(\text{Up}(F_{DB}^{i+1}), 1) \\ + \text{Conv}_1(F_{PASCA}^i, 1), 1), & i = 4, 3, 2, 1 \end{cases} \quad (22)$$

Multi-scale change masks $\{M_i\}_{i=1}^5$ are obtained by applying convolution operations on F_{DB}^i . The initial change

Table 1
Dataset details.

Dataset	Image pairs	Resolution	Train/Test	Change ratio	Categories
VL-CMU-CD	1362	1024 × 768 × 3	16005/332	0.0716	bins, signs, vehicles, maintenance, etc.
PCD	200	1024 × 224 × 3	8000/120	0.2587	trees, buildings, vehicles, etc.
CDnet	50209	320 × 240 × 3, 720 × 576 × 3	40148/10061	0.0479	person, vehicles, boats, etc.
LEVIR-CD	637	1024 × 1024 × 3	18015/4674	0.1116	buildings
CDD	11	4725 × 2700 × 3, 1900 × 1000 × 3	12998/3000	0.1234	building, vehicles, roads, etc.

map \hat{M} is generated by concatenating and convolving features M_5 , M_4 and M_3 . The final change map M is produced by integrating \hat{M} with M_2 and M_1 . The process is formulated as follows:

$$M_i = \text{Conv}_2(F_{DB}^i, 3, 1), i = 5, 4, 3, 2, 1 \quad (23)$$

$$\hat{M} = \text{Conv}_1([M_5, M_4, M_3], 1) \quad (24)$$

$$M = \text{Conv}_1([\hat{M}, M_2, M_1], 1) \quad (25)$$

The final change map M can accurately identify changes.

3.5. Loss Function

Our method formulates change detection as a binary classification task, aiming to identify whether a target object has undergone changes while disregarding semantic categories. We employ the cross-entropy loss function to quantify the pixel-wise prediction errors:

$$\mathcal{L}_{ce} = -([y \ln(p) + (1 - y) \ln(1 - p)]) \quad (26)$$

where $y \in \{0, 1\}$ denotes the ground truth, and p represents the predicted probability.

To ensure multi-scale consistency and refine predictions progressively, the total loss integrates supervision from three sources: intermediate multi-scale masks, initial change map and final change map. The total loss function is:

$$\mathcal{L}_{\text{Total}} = \mathcal{L}_{ce}(\hat{M}, M_{GT}) + \mathcal{L}_{ce}(M, M_{GT}) + \sum_{i=1}^5 \mathcal{L}_{ce}(M_i, M_{GT}) \quad (27)$$

Here, M_{GT} is the ground-truth. All intermediate masks are bilinearly upsampled to the resolution of M_{GT} .

4. Experiments

4.1. Experimental Setups

4.1.1. Datasets

We conduct experiments on three common street-view CD datasets (VL-CMU-CD, PCD, and CDnet) and two remote sensing CD datasets (LEVIR-CD and CDD). Table. 1 summarizes the details of these datasets.

- **VL-CMU-CD** [1]: Contains 1362 image pairs images in Pennsylvania, USA, from 152 real-world sequences with annotations. The resolution is 1024 × 768 pixels.
- **PCD** [19]: A panoramic CD dataset with “TSUNAMI” and “GSV” subsets. “TSUNAMI” has 100 pairs of pre- and post- Japanese tsunami panoramic images with change maps. “GSV” has 100 pairs of Google street-view panoramic images. The resolution is 1024 × 224 pixels.
- **CDnet** [35]: Consists of nearly 50000 images from 31 video sequences, shot by various sensors. The resolution ranges from 320 × 240 to 720 × 480. It covers indoor and outdoor scenes and is divided into six challenge types.
- **LEVIR-CD** [5]: Includes 637 VHR image pairs of 1024 × 1024 pixels from 20 USA regions. It covers various buildings and records over 31000 change instances.
- **CDD** [18]: Contains VHR aerial images from 11 regions including New Zealand and multiple cities. The resolution ranges from 1900 × 1000 to 4725 × 2700 pixels.

In line with IDET [14], we partition the five datasets, perform data augmentation, and resize street-view images to 320 × 320 pixels and remote sensing images to 256 × 256 pixels for training and testing.

4.1.2. Baselines

We compare our method with sixteen existing CD methods: FCNCD [22], ADCDnet [17], CSCDnet [28], IFN [38], BIT [6], STANet [5], SNUNet [10], ChangeFormer [4], TinyCD [8], Changer [11], ARCDNet [20], SGSLN [41], STENet [27], DGMA²-Net [37], DDLNet [24], and IDET [14]. Their descriptions are as follows:

- **FCNCD**: First concatenates two images into a single six-channel image, then processes it through a fully convolutional network for change detection.

- ADCDnet: Uses a Siamese network for multi-scale feature extraction. Corresponding features are subtracted to obtain difference features, which are then fused hierarchically to generate change detection results.
- CSCDnet: Extracts multi-level features via a Siamese network, estimates optical flow between images using an optical flow estimation network to align features, and performs hierarchical fusion and alignment for change detection.
- IFN: Concatenates feature pairs from a Siamese network along the channel dimension, then predicts changes using a difference discrimination network similar to a fully convolutional network.
- BIT: Extracts image pair features via a CNN-based Siamese network, then employs Transformer encoders and decoders to learn semantic tokens for enhancing original features. The enhanced features are differenced to detect changes.
- STANet: Processes raw features using spatio-temporal attention modules to interactively leverage channel-wise semantic information and spatial positional information, then discriminates change maps via distance metrics.
- SNUNet: A densely connected Siamese network combining Siamese architecture and nested U-Net, integrating channel attention mechanisms to fuse and refine multi-level semantic features under deep supervision for more precise change detection.
- ChangeFormer: Adopts hierarchical Transformer encoders for feature extraction. The concatenated change features are fused through a multi-layer perceptron (MLP) to generate the final change map.
- TinyCD: A lightweight change detection network based on Siamese U-Net and EfficientNet [32]. It employs hybrid strategies for feature fusion to obtain difference features and uses MLPs for pixel-level classification.
- Changer: Processes feature alignment during feature extraction using interactive strategies like aggregated distributions and feature swapping, while introducing a flow-based dual alignment fusion module for effective alignment and feature fusion.
- ARCDNet: Employs knowledge review modules to mine multi-level temporal differences, integrates on-line uncertainty estimation for uncertainty-aware learning, and fuses these features to generate change maps.
- SGSLN: A binary change detection method with an exchanging dual encoder-decoder structure, integrating semantic guidance and spatial localization to address bitemporal feature fusion at decision level and semantic-guided change area identification.
- STENet: A dual encoder-decoder method integrating semantic-spatial cues to address decision-layer fusion and semantic-driven detection in bitemporal change analysis.
- DGMA²-Net: A difference-guided multiscale aggregation network leveraging multiscale difference fusion, difference aggregation modules, and difference-attention refinement for change feature optimization.
- DDLNet: A dual-domain (frequency/spatial) RSCD network leveraging frequency enhancement to amplify critical changes and spatial detail fusion to recover fine-grained spatiotemporal features, enabling robust change detection.
- IDET: Extracts features via a CNN-based Siamese network, iteratively enhances original and change features using a Transformer structure, and progressively fuses enhanced change features from coarse to fine for detection.

All methods are implemented with PyTorch and trained on the same datasets.

4.1.3. Implementation Details

The experiments are implemented with PyTorch and trained on a single NVIDIA GeForce 2080Ti GPU. We adopt the Adam optimizer with an initial learning rate of 1e-3, a momentum of 0.9, and a weight decay of 0.999. The batch size is configured to 4. All methods are trained for 20 epochs on three common street-view CD datasets and 200 on two remote sensing CD datasets.

4.1.4. Evaluation Metrics

To accurately evaluate the performance of different methods, we adopt five commonly used evaluation metrics: Precision (P), Recall (R), F1-measure ($F1$), Overall Accuracy (OA), and Intersection over Union (IoU). The formulas are as follows:

$$P = \frac{TP}{TP + FP} \quad (28)$$

$$R = \frac{TP}{TP + FN} \quad (29)$$

$$F1 = \frac{2 \times P \times R}{P + R} \quad (30)$$

$$OA = \frac{TP + TN}{TP + TN + FP + FN} \quad (31)$$

$$IoU = \frac{TP}{TP + FP + FN} \quad (32)$$

where TP , TN , FP , and FN denote true positive, true negative, false positive, and false negative, respectively. Higher $F1$ and IoU values indicate better-performing methods, as they reflect more accurate positive-sample identification and better overlap between predicted and actual results.

Table 2

Quantitative comparison of different CD methods on VL-CMU-CD, PCD and CDnet datasets. Note that **red** marks the best-performing method, **blue** the second-best, and **green** the third-best.

Method	VL-CMU-CD					PCD					CDnet				
	<i>P</i>	<i>R</i>	<i>F1</i>	<i>OA</i>	<i>IoU</i>	<i>P</i>	<i>R</i>	<i>F1</i>	<i>OA</i>	<i>IoU</i>	<i>P</i>	<i>R</i>	<i>F1</i>	<i>OA</i>	<i>IoU</i>
FCNCD	84.2	84.3	84.2	98.4	72.9	68.7	61.7	65.0	94.1	48.0	82.9	88.3	85.5	99.2	76.0
ADCDnet	92.8	94.3	93.5	99.3	87.9	78.8	73.4	76.0	90.0	62.3	89.0	85.5	87.2	99.3	77.9
CSCDnet	89.2	91.1	90.1	98.7	82.1	66.0	72.6	69.1	83.7	51.9	93.9	82.3	87.7	99.0	78.4
IFN	93.1	75.9	83.6	98.1	71.4	69.5	75.7	72.5	87.2	57.7	93.1	80.0	86.1	98.9	75.3
BIT	90.5	87.6	89.0	98.8	80.6	77.7	57.3	66.0	85.4	50.1	95.4	81.9	88.1	99.1	78.9
STANet	73.1	95.8	82.9	98.0	70.7	69.6	52.7	60.0	79.9	41.2	72.2	94.3	81.8	98.3	69.2
SNUNet	78.4	83.1	80.7	97.9	67.7	73.7	67.5	70.5	86.9	54.8	91.8	88.4	90.1	99.4	82.0
ChangeFormer	88.0	88.6	88.3	98.7	79.2	74.0	69.2	71.5	86.6	56.4	93.4	85.9	89.5	99.2	81.3
TinyCD	89.4	94.2	91.8	99.1	85.0	67.6	83.2	74.6	85.7	58.9	90.0	93.8	91.9	99.5	84.9
Changer	93.1	90.7	91.9	99.2	85.1	73.4	64.2	68.5	86.5	52.7	95.7	89.7	92.6	99.6	87.2
ARCDNet	76.3	97.5	85.6	98.4	74.8	67.2	78.9	72.3	89.2	60.8	74.7	94.4	83.4	98.4	71.8
SGSLN	74.0	97.5	84.2	98.2	72.7	68.3	80.7	74.0	87.8	62.1	75.8	93.0	83.5	98.5	72.0
STENet	89.1	80.5	84.6	98.4	73.6	72.0	74.5	73.2	87.3	57.8	77.0	88.6	82.4	98.4	70.6
DGMA ² -Net	89.2	92.9	91.0	99.1	83.8	68.5	76.1	72.1	86.3	56.4	77.6	92.4	84.3	98.6	73.3
DDLNet	88.6	94.8	91.6	99.2	84.5	77.0	68.5	72.5	88.9	57.9	85.4	90.7	88.0	99.0	79.0
IDET	93.5	94.5	94.0	99.4	88.7	74.2	77.9	76.0	88.8	61.9	90.8	94.1	92.4	99.7	86.2
CEBSNet (Ours)	93.0	95.5	94.2	99.4	89.1	79.2	74.8	76.9	90.1	63.0	93.1	95.5	94.3	99.7	89.1

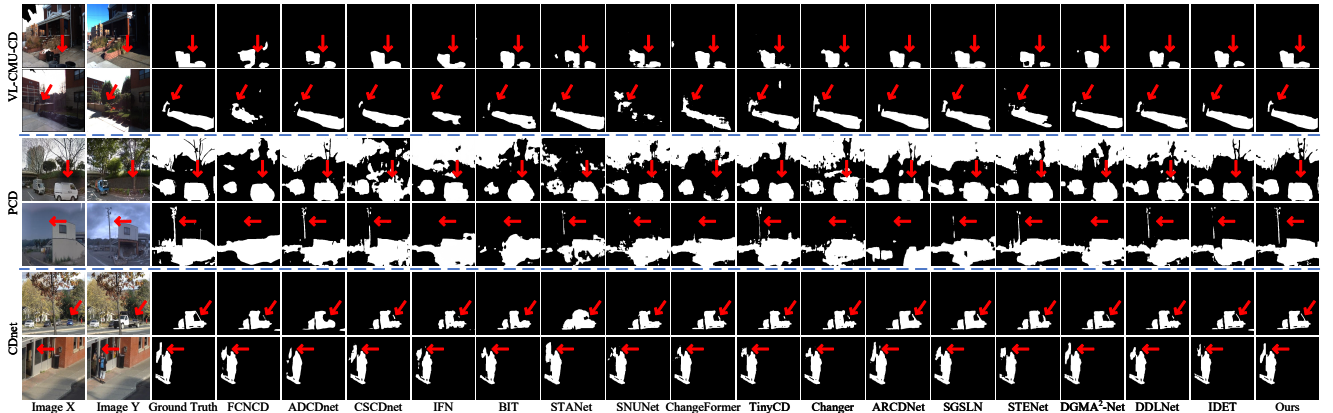


Figure 8: Detection results of different methods on VL-CMU-CD, PCD, and CDnet datasets. The **red arrows** indicate noticeable changes.

4.2. Main Results

4.2.1. Results on Common Street-view CD Datasets

Table 2 presents the experimental results of our method and other comparative methods on three common street-view datasets, namely VL-CMU-CD, PCD, and CDnet. These results clearly show that our CEBSNet achieves the best performance across all three datasets, validating its generalizability in complex street-view scenarios. On VL-CMU-CD, our CEBSNet achieves the peak performance in *F1*, *OA*, and *IoU* metrics, reaching 94.2%, 99.4%, and 89.1% respectively. When compared with the previous SOTA method IDET, the *F1* and *IoU* values are improved by 0.2% and 0.4% respectively. For PCD dataset, which contains highly challenging scenarios with diverse changes (e.g., buildings, trees, grasslands, vehicles), our method attains the highest *P* (79.2%), *F1* (76.9%), and *IoU* (63.0%).

Notably, its *F1* score is 0.9% higher than ADCDnet and IDET, indicating its effectiveness in handling complex changes. On CDnet, our CEBSNet excels in four metrics: *R* (95.5%), *F1* (94.3%), *OA* (99.7%), and *IoU* (89.1%). Compared with Changer, these metrics are increased by 5.8%, 1.7%, 0.1%, and 1.9% respectively, further validating its superiority. These results firmly prove that our CEBSNet excels in common street-view change detection, showing its great potential for real-world applications.

Fig. 8 shows some typical examples of different methods on three common street-view datasets. Accurate and complete detection is crucial for identifying main change areas and handling details and noise. Most methods can detect main change regions, but struggle with details and background noise. Methods like FCNCD, IFN, Changer, STENet, and DDLNet tend to lose details when capturing

Table 3

Quantitative comparison of different CD methods on LEVIR-CD and CDD datasets. Note that **red** marks the best-performing method, **blue** the second-best, and **green** the third-best.

Method	LEVIR-CD					CDD				
	<i>P</i>	<i>R</i>	<i>F1</i>	<i>OA</i>	<i>IoU</i>	<i>P</i>	<i>R</i>	<i>F1</i>	<i>OA</i>	<i>IoU</i>
FCNCD	89.7	84.0	86.8	97.7	77.1	85.1	69.8	76.7	97.5	63.7
ADCDnet	90.4	81.8	85.9	97.4	75.4	92.5	78.8	85.1	98.5	75.1
CSCDnet	84.6	81.6	83.1	96.8	71.5	79.1	48.9	60.4	90.9	42.7
IFN	89.7	79.8	84.5	96.9	72.7	94.2	69.2	79.8	97.7	66.5
BIT	92.1	81.6	86.5	97.7	76.3	93.5	80.2	86.3	98.7	76.6
STANet	84.8	69.9	76.6	95.3	61.8	71.6	69.6	70.6	95.0	54.6
SNUNet	88.2	83.8	86.0	97.7	76.0	86.3	64.0	73.5	97.0	58.8
ChangeFormer	90.7	85.5	88.0	98.0	79.0	89.2	73.0	80.3	98.0	68.0
TinyCD	89.2	83.4	86.2	97.2	76.3	95.1	80.1	87.0	98.8	77.6
Changer	92.9	74.8	82.9	97.0	70.4	94.8	73.0	82.5	98.4	70.9
ARCDNet	91.4	86.5	88.9	97.9	80.0	81.8	83.4	82.6	97.3	71.2
SGSLN	90.8	87.5	89.2	98.1	80.8	83.6	86.7	85.1	97.8	74.9
STENet	91.7	70.4	79.7	95.6	66.4	68.5	53.0	59.7	93.9	43.0
DGMA ² -Net	90.9	70.1	79.1	95.5	65.8	73.6	77.1	75.3	97.0	61.7
DDLNet	90.9	84.4	87.5	97.7	77.8	91.6	80.2	85.5	98.5	75.3
IDET	91.3	86.6	88.9	98.1	80.2	91.1	83.1	86.9	98.7	77.6
CEBSNet (Ours)	92.7	87.2	89.9	98.2	81.8	99.1	87.1	92.7	99.3	86.5

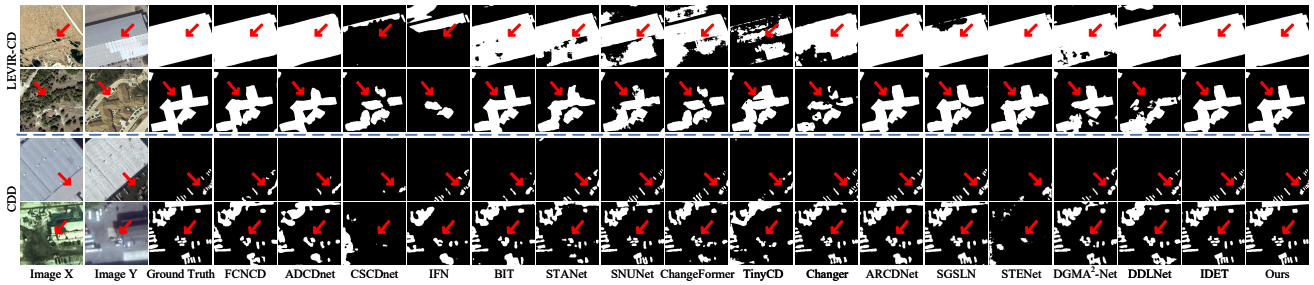


Figure 9: Detection results of different methods on LEVIR-CD and CDD datasets. The **red arrows** indicate noticeable changes.

main changes, thus affecting the judgement of changes. CSCDnet and BIT are easily interfered by the background noise, causing detection errors and inaccurate marking of change areas. STANet, SNUNet, and ChangeFormer are severely affected by background noise, sometimes even missing main change objects, resulting in incomplete and unreliable results. Among these methods, ADCDnet and IDET perform relatively better. But due to background noise from large time spans, they ignore the subtle changes. Our method has distinct advantages. It can accurately detect change regions, keep rich details, and cover both significant and subtle changes, like large-scale building renovation or subtle road-sign alterations. This shows its higher accuracy and stronger robustness, further validating its superior performance in common street-view change detection.

4.2.2. Results on Remote Sensing CD Datasets

Table 3 presents the experimental results of our method and other comparative methods on two remote sensing datasets, namely LEVIR-CD and CDD. These results clearly demonstrate that our method achieves the optimal performance on both datasets, confirming its effectiveness in complex remote sensing scenarios. On LEVIR-CD, our

CEBSNet attains the best results in *F1*, *OA*, and *IoU* metrics, reaching 89.9%, 98.2%, and 81.8% respectively. Compared with the previously best-performing SGSLN, our method shows improvements of 0.7%, 0.1%, and 1.0% in these metrics. On CDD, our CEBSNet outperforms other methods in all five metrics of *R*, *P*, *F1*, *OA*, and *IoU*, with specific values of 99.1%, 87.1%, 92.7%, 99.3%, and 86.5% respectively. Notably, CEBSNet is the only method with an *F1* score exceeding 90.0%. When compared with TinyCD, our method shows significant improvements in all these five metrics, with the increments being 4.3%, 5.7%, 0.5%, and 8.9% respectively. These findings clearly show our method's outstanding performance and its great potential in remote sensing change detection.

Fig. 9 shows some typical examples of different methods on two remote sensing datasets. In the 1st and 2nd rows, methods like ADCDnet, ARCDNet, SGSLN, IDET, and our CEBSNet can comprehensively detect building changes. Conversely, the remaining methods encounter issues like non-detection or partial detection failures, failing to accurately represent building change information. In the 3rd and 4th rows, ARCDNet, SGSLN, DGMA²-Net, and our CEBSNet can precisely capture detailed information. when

Table 4

Comparison of computational costs and parameter counts on common street-view datasets.

Method	GFLOPs	Params (M)
FCNCD	100.2	134.2
ADCDnet	217.6	32.2
CSCDnet	65.9	92.3
IFN	128.5	50.4
BIT	53.8	3.4
STANet	20.1	16.8
SNUNet	85.7	12.0
ChangeFormer	316.9	29.7
TinyCD	2.4	0.27
Changer	9.1	11.3
ARCDNet	22.1	14.3
SGSLN	18.0	6.0
STENet	28.6	37.1
DGMA ² -Net	23.0	11.0
DDLNet	11.3	12.7
IDET	195.9	100.7
CEBSNet (Ours)	174.7	86.0

confronted with minuscule and dispersed change regions, most methods are highly susceptible to noise interference. This lead to miss minor changes, causing false positives and false negatives. Among all these methods, our CEBSNet showcases remarkable advantages in both accuracy and integrity. It can accurately identify main change regions and clearly reveal fine-grained details. Even for subtle change areas, it still yield satisfactory detection results. The visual evidence aligns with quantitative metrics, confirming the effectiveness and robustness of our CEBSNet in complex remote sensing change detection.

4.2.3. Computational Complexity Analysis

Table 4 shows the computational costs and parameter counts across different methods on common street-view datasets with an image size of 320×320 . By conducting an in-depth comparison of the performance and complexity of each method, our method achieves the best performance across all datasets while maintaining appropriate costs in GFLOPs and Params. In terms of GFLOPs, our method exhibits lower computational complexity than methods like ADCDnet and IDET. Regarding Params, it requires fewer parameters than networks such as FCNCD, CSCDnet, and IDET. In conclusion, our method strikes a good balance between complexity and performance, enabling excellent detection performance with moderate complexity.

4.3. Ablation Studies

In this section, we conduct three ablation experiments and one feature visualization analysis to thoroughly evaluate the key components and performance of our method. We begin by exploring the main components' impact on performance. Then, we analyze the optimal feature shift ratio in Channel Swap Module (CSM) for better temporal correlation modeling. After that, we study the k -value setting

Table 5

Ablation study with varying components on VL-CMU-CD dataset. Best metrics are highlighted in **bold**.

Base	CSM	CGFF	FESM	PASCA	P	R	$F1$	OA	IoU
✓					91.36	94.63	92.96	99.23	86.85
✓	✓				91.88	95.78	93.79	99.33	88.35
✓	✓	✓			92.51	95.34	93.90	99.35	88.58
✓	✓	✓	✓		92.88	95.29	94.07	99.36	88.48
✓	✓	✓	✓	✓	92.96	95.47	94.20	99.36	89.08

Note: Components marked with ✓ are activated. Abbreviations: CSM (Channel Swap Module), CGFF (Change-Guided Feature Fusion), FESM (Feature Excitation and Suppression Module), PASCA (Pyramid-Aware Spatial-Channel Attention).

Table 6

Ablation Analysis of feature shift ratio in CSM. Best scores in **bold**.

Ratio	P	R	$F1$	OA	IoU
0	91.32	95.38	93.31	99.29	87.53
1/4	92.96	95.47	94.20	99.36	89.08
2/4	92.67	95.68	94.15	99.36	88.99
3/4	92.20	95.92	94.03	99.35	88.73
4/4	93.06	94.90	93.97	99.37	88.65

in Feature Excitation and Suppression Module (FESM). Finally, a feature visualization analysis is performed to shows each module's response during feature processing. Note that all ablation studies are conducted on VL-CMU-CD dataset.

4.3.1. Component Effectiveness Analysis

To thoroughly evaluate the contribution of each component in our method, we conduct a series of ablation experiments using a module-combination strategy. The experimental results on VL-CMU-CD dataset are presented in Table 5, clearly showing the performance gains with different module combinations. The CSM enhances the network's noise resilience by modeling the temporal dependencies between image pairs. The CGFF enriches difference information with global context. The FESM improves the detection accuracy of change regions through excitation and suppression operations. The PASCA employs its multi-receptive fields and attention mechanism, contributing to more accurate change detection. In summary, the ablation results prove the rational design and effectiveness of each module in enhancing network performance, highlighting their importance.

4.3.2. Impact of Channel Shift Ratio in CSM

Table 6 evaluates the channel shift ratio in Channel Swap Module (CSM), quantifying its impact. Our experiments with swap ratios $\{0, 1/4, 2/4, 3/4, 4/4\}$ reveal that a 1/4 ratio achieves peak performance on VL-CMU-CD, motivating its adoption as the default configuration. The experiments indicate that moderate feature interaction enhances temporal correlation modeling and noise suppression, whereas excessive swapping degrades dependency learning. The 1/4 balance preserves discriminative spatio-temporal patterns while mitigating redundancy.

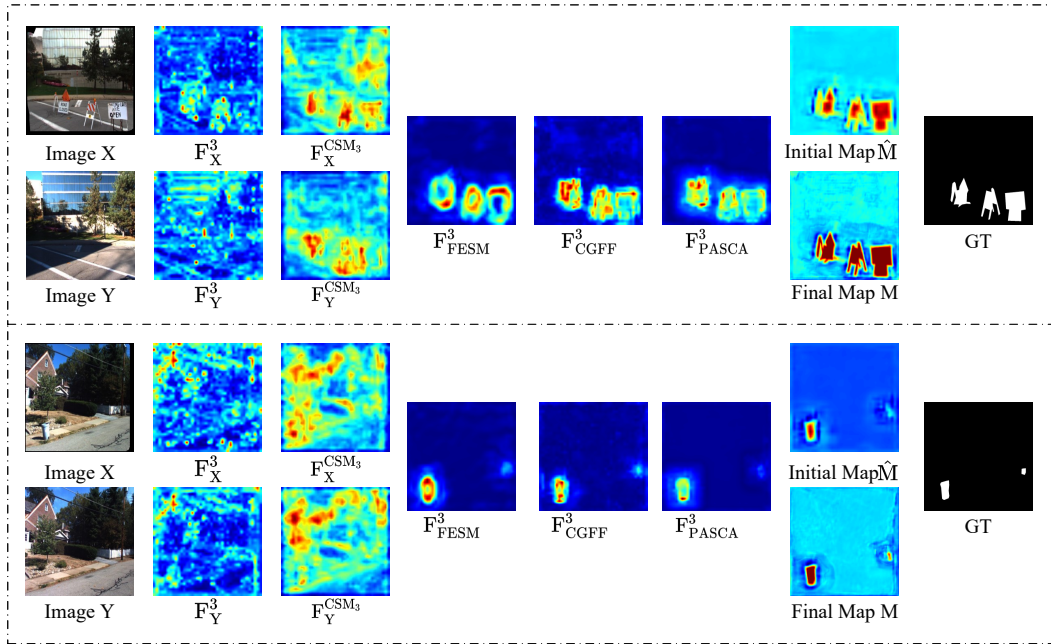


Figure 10: Progressive feature refinement through key modules: Visualization results showing the effects of CSM, FESM, CGFF, and PASCA on image features and final change map compared with the ground truth.

Table 7

Ablation analysis on k configurations in FESM. Best scores in **bold**.

Type	$\{k_4, k_3, k_2, k_1\}$	P	R	$F1$	OA	IoU
Dynamic	$\{2, 4, 8, 16\}$	92.98	95.02	93.99	99.36	88.69
	$\{4, 8, 16, 32\}$	92.54	95.49	93.99	99.38	88.70
	$\{5, 10, 20, 40\}$	92.96	95.47	94.20	99.36	89.08
Fixed	$\{4, 4, 4, 4\}$	92.57	95.48	94.00	99.37	88.71
	$\{5, 5, 5, 5\}$	92.31	95.50	93.88	99.36	88.49
	$\{10, 10, 10, 10\}$	92.86	95.37	94.10	99.36	88.91

subsubsectionImpact of Hierarchical k -value Configuration in FESM Table 7 details the setting of the k -value in Feature Excitation and Suppression Module (FESM). To explore its impact on model performance, we conduct two controlled experiments:

- **Dynamic- k Group:** Fix pixel span to 4 while assigning layer-specific k -values (network levels $i = 4, 3, 2, 1$).
- **Fixed- k Group:** Maintain identical k -values across layers with adaptive pixel spans.

On VL-CMU-CD, the dynamic- k configuration with values $\{5, 10, 20, 40\}$ achieves peak performance with 94.20% $F1$ and 89.08% IoU , outperforming fixed- k baselines by 0.21% - 0.59% $F1$ points. This verifies that progressively increasing k -values in deeper layers (from $i = 4$ to $i = 1$) enhance multi-scale feature discrimination, whereas uniform k -values cause either oversuppression (small k) or noisy activation (large k). We therefore adopt $\{5, 10, 20, 40\}$ as default configuration.

4.3.3. Module-Wise Feature Visualization Analysis

Fig. 10 illustrates the progressive refinement of features through our key modules. The initial siamese features reveal significant inter-image discrepancies, which are effectively suppressed by the CSM while preserving structural coherence. For change feature refinement, FESM selectively amplifies subtle changes, while CGFF integrates complementary patterns, jointly enhancing boundary precision. Spatial Refinement is achieved through PASCA, which captures multiscale context and enables pixel-wise localization of changes at varying scales. The initial change map is refined via attention-guided edge sharpening and multiscale feature fusion, yielding final map \mathbf{M} that closely align with ground truth \mathbf{GT} , balancing holistic accuracy and granular fidelity.

5. Conclusion

In this paper, we propose CEBSNet, a novel change detection framework designed to mitigate the critical challenges of noise interference and subtle-change neglect in complex scenarios. By integrating the Channel Swap Module, our method effectively models temporal dependencies between image pairs, reducing inter-pair discrepancies and enhancing robustness against illumination, seasonal variations, and other noise factors. The Feature Excitation and Suppression Module further improves detection accuracy by emphasizing change-related regions while suppressing background distractions. Additionally, the Pyramid-Aware Spatial-Channel Attention module leverages multi-scale receptive fields and spatio-channel attention to capture changes of diverse sizes, ensuring comprehensive detection performance. Extensive experiments on three common street-view and two remote sensing datasets demonstrate that

CEBSNet outperforms sixteen state-of-the-art methods. Future efforts will focus on lightweight deployment strategies to balance computational efficiency and detection accuracy.

Authorship contribution statement

Conceptualization, Q.X. and Y.X.; methodology, Q.X. and Y.X.; software, Q.X. and J.H.; validation, Q.X. and J.H.; formal analysis, Q.X.; investigation, Q.X. and R.H.; resources, Q.X. and Y.X.; data curation, Q.X.; writing—original draft preparation, Q.X. and Y.J.; writing—review and editing, Q.X., Y.X. and R.H.; visualization, Y.J.; supervision, Y.X.; project administration, R.H.; funding acquisition, Y.X. and R.H.. All authors have read and agreed to the published version of the manuscript.

Funding

This research was funded by the Scientific Research Program of Tianjin Municipal Education Commission 2023KJ232 and the Tianjin Natural Science Foundation General Project 24JCYBJC00990.

References

- [1] Pablo F Alcantarilla, Simon Stent, German Ros, Roberto Arroyo, and Riccardo Gherardi. Street-view change detection with deconvolutional networks. *Autonomous Robots*, 42:1301–1322, 2018.
- [2] Anju Asokan and JJESI Anitha. Change detection techniques for remote sensing applications: A survey. *Earth Science Informatics*, 12:143–160, 2019.
- [3] Ting Bai, Le Wang, Dameng Yin, Kaimin Sun, Yepi Chen, Wenzhuo Li, and Deren Li. Deep learning for change detection in remote sensing: a review. *Geo-spatial Information Science*, 26(3):262–288, 2023.
- [4] Wele Gedara Chaminda Bandara and Vishal M Patel. A transformer-based siamese network for change detection. In *IGARSS 2022-2022 IEEE International Geoscience and Remote Sensing Symposium*, pages 207–210. IEEE, 2022.
- [5] Hao Chen and Zhenwei Shi. A spatial-temporal attention-based method and a new dataset for remote sensing image change detection. *Remote sensing*, 12(10):1662, 2020.
- [6] Hao Chen, Zipeng Qi, and Zhenwei Shi. Remote sensing image change detection with transformers. *IEEE Transactions on Geoscience and Remote Sensing*, 60:1–14, 2021.
- [7] Guangliang Cheng, Yunmeng Huang, Xiangtai Li, Shuchang Lyu, Zhaoyang Xu, Hongbo Zhao, Qi Zhao, and Shiming Xiang. Change detection methods for remote sensing in the last decade: A comprehensive review. *Remote Sensing*, 16(13):2355, 2024.
- [8] Andrea Codegoni, Gabriele Lombardi, and Alessandro Ferrari. Tinycd: A (not so) deep learning model for change detection. *Neural Computing and Applications*, 35(11):8471–8486, 2023.
- [9] Rodrigo Caye Daudt, Bertr Le Saux, and Alexandre Boulch. Fully convolutional siamese networks for change detection. In *2018 25th IEEE international conference on image processing (ICIP)*, pages 4063–4067. IEEE, 2018.
- [10] Sheng Fang, Kaiyu Li, Jinyuan Shao, and Zhe Li. Snunet-cd: A densely connected siamese network for change detection of vhr images. *IEEE Geoscience and Remote Sensing Letters*, 19:1–5, 2021.
- [11] Sheng Fang, Kaiyu Li, and Zhe Li. Changer: Feature interaction is what you need for change detection. *IEEE Transactions on Geoscience and Remote Sensing*, 61:1–11, 2023.
- [12] Yuchao Feng, Jiawei Jiang, Honghui Xu, and Jianwei Zheng. Change detection on remote sensing images using dual-branch multilevel intertemporal network. *IEEE Transactions on Geoscience and Remote Sensing*, 61:1–15, 2023.
- [13] Jun Fu, Jing Liu, Haijie Tian, Yong Li, Yongjun Bao, Zhiwei Fang, and Hanqing Lu. Dual attention network for scene segmentation. In *Proceedings of the IEEE/CVF conference on computer vision and pattern recognition*, pages 3146–3154, 2019.
- [14] Qing Guo, Ruofei Wang, Rui Huang, Renjie Wan, Shuifa Sun, and Yuxiang Zhang. Idet: Iterative difference-enhanced transformers for high-quality change detection. *IEEE Transactions on Emerging Topics in Computational Intelligence*, 2025.
- [15] Shima Holail, Tamer Saleh, Xiongwu Xiao, Jing Xiao, Gui-Song Xia, Zhenfeng Shao, Jianya Gong, and Deren Li. Time-series satellite remote sensing reveals gradually increasing war damage in the gaza strip. *National Science Review*, 11(9):nwae304, 08 2024. ISSN 2095-5138. doi: 10.1093/nsr/nwae304. URL <https://doi.org/10.1093/nsr/nwae304>.
- [16] Jie Hu, Li Shen, and Gang Sun. Squeeze-and-excitation networks. In *Proceedings of the IEEE conference on computer vision and pattern recognition*, pages 7132–7141, 2018.
- [17] Rui Huang, Mo Zhou, Qiang Zhao, and Yaobin Zou. Change detection with absolute difference of multiscale deep features. *Neurocomputing*, 418:102–113, 2020.
- [18] Shunping Ji, Shiqing Wei, and Meng Lu. Fully convolutional networks for multisource building extraction from an open aerial and satellite imagery data set. *IEEE Transactions on geoscience and remote sensing*, 57(1):574–586, 2018.
- [19] CREST JST. Change detection from a street image pair using cnn features and superpixel segmentation. In *Proceedings of the British Machine Vision Conference*, page 61, 2015.
- [20] Zhenglai Li, Chang Tang, Xianju Li, Weiying Xie, Kun Sun, and Xinzhong Zhu. Towards accurate and reliable change detection of remote sensing images via knowledge review and online uncertainty estimation. *arXiv e-prints*, pages arXiv–2305, 2023.
- [21] Zhenglai Li, Chang Tang, Xinwang Liu, Wei Zhang, Jie Dou, Lizhe Wang, and Albert Y Zomaya. Lightweight remote sensing change detection with progressive feature aggregation and supervised attention. *IEEE Transactions on Geoscience and Remote Sensing*, 61:1–12, 2023.
- [22] Jonathan Long, Evan Shelhamer, and Trevor Darrell. Fully convolutional networks for semantic segmentation. In *Proceedings of the IEEE conference on computer vision and pattern recognition*, pages 3431–3440, 2015.
- [23] Zhiyong Lv, Pingdong Zhong, Wei Wang, Zhenzhen You, and Nicola Falco. Multiscale attention network guided with change gradient image for land cover change detection using remote sensing images. *IEEE Geoscience and Remote Sensing Letters*, 20:1–5, 2023.
- [24] Xiaowen Ma, Jiawei Yang, Rui Che, Huang Zhang, and Wei Zhang. Ddlnet: Boosting remote sensing change detection with dual-domain learning. In *2024 IEEE International Conference on Multimedia and Expo (ICME)*, pages 1–6. IEEE, 2024.
- [25] Zhaoyang Niu, Guoqiang Zhong, and Hui Yu. A review on the attention mechanism of deep learning. *Neurocomputing*, 452:48–62, 2021.
- [26] Jun Pan, Yuchuan Bai, Qidi Shu, Zhuoer Zhang, Jiarui Hu, and Mi Wang. M-swin: Transformer-based multi-scale feature fusion change detection network within cropland for remote sensing images. *IEEE Transactions on Geoscience and Remote Sensing*, 2024.
- [27] Xiang Pan, Jintao Lai, Yiting Jin, Xiaolei Zhou, and Jianwei Zheng. Stenet: A spatial selection and temporal evolution network for change detection in remote sensing images. *IEEE Transactions on Geoscience and Remote Sensing*, 62:1–15, 2024.
- [28] Ken Sakurada, Mikiya Shibuya, and Weimin Wang. Weakly supervised silhouette-based semantic scene change detection. In *2020 IEEE International conference on robotics and automation (ICRA)*, pages 6861–6867. IEEE, 2020.
- [29] Ayesha Shafique, Guo Cao, Zia Khan, Muhammad Asad, and Muhammad Aslam. Deep learning-based change detection in remote sensing images: A review. *Remote Sensing*, 14(4):871, 2022.

- [30] Wenzhong Shi, Min Zhang, Rui Zhang, Shanxiong Chen, and Zhao Zhan. Change detection based on artificial intelligence: State-of-the-art and challenges. *Remote Sensing*, 12(10):1688, 2020.
- [31] Qi Song, Jie Li, Chenghong Li, Hao Guo, and Rui Huang. Fully attentional network for semantic segmentation. In *Proceedings of the AAAI Conference on Artificial Intelligence*, volume 36, pages 2280–2288, 2022.
- [32] Mingxing Tan and Quoc Le. Efficientnet: Rethinking model scaling for convolutional neural networks. In *International conference on machine learning*, pages 6105–6114. PMLR, 2019.
- [33] Aparna Taneja, Luca Ballan, and Marc Pollefeys. Image based detection of geometric changes in urban environments. In *2011 international conference on computer vision*, pages 2336–2343. IEEE, 2011.
- [34] Ashish Vaswani, Noam Shazeer, Niki Parmar, Jakob Uszkoreit, Llion Jones, Aidan N Gomez, Łukasz Kaiser, and Illia Polosukhin. Attention is all you need. *Advances in neural information processing systems*, 30, 2017.
- [35] Yi Wang, Pierre-Marc Jodoin, Fatih Porikli, Janusz Konrad, Yannick Benezeth, and Prakash Ishwar. Cdnet 2014: An expanded change detection benchmark dataset. In *Proceedings of the IEEE conference on computer vision and pattern recognition workshops*, pages 387–394, 2014.
- [36] Sanghyun Woo, Jongchan Park, Joon-Young Lee, and In So Kweon. Cbam: Convolutional block attention module. In *Proceedings of the European conference on computer vision (ECCV)*, pages 3–19, 2018.
- [37] Zilu Ying, Zijun Tan, Yikui Zhai, Xudong Jia, Wenba Li, Junying Zeng, Angelo Genovese, Vincenzo Piuri, and Fabio Scotti. Dgma 2-net: a difference-guided multiscale aggregation attention network for remote sensing change detection. *IEEE Transactions on Geoscience and Remote Sensing*, 2024.
- [38] Chenxiao Zhang, Peng Yue, Deodato Tapete, Liangcun Jiang, Boyi Shangguan, Li Huang, and Guangchao Liu. A deeply supervised image fusion network for change detection in high resolution bi-temporal remote sensing images. *ISPRS Journal of Photogrammetry and Remote Sensing*, 166:183–200, 2020.
- [39] Xiaofeng Zhang, Shuli Cheng, Liejun Wang, and Haojin Li. Asymmetric cross-attention hierarchical network based on cnn and transformer for bitemporal remote sensing images change detection. *IEEE Transactions on Geoscience and Remote Sensing*, 61:1–15, 2023.
- [40] Feng Zhao, Zhenglin Zhu, Hanqiang Liu, and Junjie Zhang. Multi-scale alignment and progressive feature fusion network for high resolution remote sensing images change detection. *IEEE Transactions on Geoscience and Remote Sensing*, 2024.
- [41] Sijie Zhao, Xueliang Zhang, Pengfeng Xiao, and Guangjun He. Exchanging dual-encoder–decoder: A new strategy for change detection with semantic guidance and spatial localization. *IEEE Transactions on Geoscience and Remote Sensing*, 61:1–16, 2023.